Onset Mechanism of Strain-Rate-Induced Flow Stress Upturn

Yue Fan,[1] Yuri N. Osetsky,[3] Sidney Yip,[1,2] and Bilge Yildiz[1,*]

[1]Department of Nuclear Science and Engineering

[2]Department of Materials Science and Engineering, Massachusetts Institute of Technology, 77 Massachusetts Avenue, Cambridge, Massachusetts, 02139, USA

[3]Materials Science and Technology Division, Oak Ridge National Laboratory, Oak Ridge, Tennessee 37831, USA

(Received 30 June 2012; published 28 September 2012)

The strain-rate response of flow stress in a plastically deforming crystal is formulated through a stress-sensitive dislocation mobility model that can be evaluated by atomistic simulation. For the flow stress of a model crystal of bcc Fe containing a $\frac{1}{2}\langle 111\rangle$ screw dislocation, this approach describes naturally a non-Arrhenius upturn at high strain rate, an experimentally established transitional behavior for which the underlying mechanism has not been clarified. Implications of our findings regarding the previous explanations of strain-rate effects on flow stress are discussed.

DOI: 10.1103/PhysRevLett.109.135503 PACS numbers: 62.20.F−

At low temperature, the deformation of metals is largely governed by the thermal activation of dislocation glide [1]. Experiments on different structures of metals, including Fe, Ta, Cu, Al, and Zn [1–6], indicate the dislocation flow stress varies with strain rate in an apparently universal manner. The flow stress increases slowly in an Arrhenius manner at low strain rates but turns upward sharply beyond a certain range of strain rate. Although the results for different metals can be quantitatively different, the flow stress "upturn" behavior when the strain rate reaches the range of 10^3–10^4 s^{-1} [6,7] appears to have a more fundamental origin. The onset of non-Arrhenius response has elicited the development of several empirical constitutive models [1,7–14], including the assumption of phonon drag effects to account for the data at high strain rates. All existing models to date use adjustable parameters to connect the flow stress below and above the critical strain rate for upturn.

In this Letter, we derive a general formalism to describe the flow stress–strain rate relation by focusing on the transition time for an activated event that is both thermally and stress driven. We show that the temperature dependence of the transition time is significantly non-Arrhenius at high strain rates. When applied to predict the dislocation flow stress in single crystals, this non-Arrhenius behavior leads naturally to the experimentally observed stress upturn at high strain rate, without invoking a different physical mechanism, or introducing any bridging parameters.

The derivation of the flow stress dependence on the strain rate is described first. In the thermal activation regime, a dislocation is located on the bottom of its potential energy valley until a thermal fluctuation enables it to climb over the activation barrier to glide to the next valley. In general, the activation free energy for dislocation flow is a function of both temperature and stress, represented as $Q(\sigma, T) = (1 - T/T_m)E(\sigma)$ [15], with T_m being the melting temperature and $E(\sigma)$ the glide activation energy at 0 K. Because we will be concerned only with the low-temperature regime (less than $0.15T_m$), we can take $Q(\sigma, T) \approx E(\sigma)$. The activation energy is known to decrease with applied stress [15–19]. When a strain rate is applied, the system begins to deform as time evolves, thus the state of stress becomes time-dependent as does $E(\sigma)$. With this in mind and following the transition state theory [20], we will write the escape rate of a dislocation from the potential energy valley at a certain stress state as

$$k(\sigma) = k_0 e^{-[E(\sigma)/k_B T]}, \tag{1}$$

where k_0 is the attempt frequency. The activation barrier $E(\sigma)$ is yet to be specified. In the elastic deformation regime, the dependence of stress on applied strain rate as a function of time, t, is given by

$$\sigma = G\varepsilon = G\dot{\varepsilon}t, \tag{2}$$

where G is the shear modulus. The ε in Eq. (2) represents the elastic strain, because in this Letter we focus on the initiation of dislocation flow, which pertains to the transition from an elastic deformation regime to a plastic deformation regime. In light of Eq. (2), $k(\sigma)$ can be represented as a function of time, $k(t)$.

The residence probability $P(t)$ that the dislocation does not escape to a neighboring potential energy valley during time t (i.e., the system remains in the elastic deformation regime) is defined as [15]

$$\frac{dP(t)}{dt} = -k(t)P(t) \tag{3}$$

or

$$P(t) = \frac{1}{C}\exp\left[-\int_0^t k(t')dt'\right], \tag{4}$$

where C is the normalization factor. Accordingly, the first-escape probability distribution $p(t)$ is given by

$$p(t) = -\frac{dP(t)}{dt} = \frac{1}{C}k(t)\exp\left[-\int_0^t k(t')dt'\right], \quad (5)$$

with normalization

$$\int_0^{t_c} p(t)dt = 1 \Rightarrow C = \int_0^{t_c} k(t)\exp[-\int_0^t k(t')dt']dt, \quad (6)$$

where $t_c = \frac{\sigma_c}{G\dot{\varepsilon}}$ represents the maximum residence time, at a given nonzero strain rate $\dot{\varepsilon}$. The average residence time is therefore

$$\bar{t} = \int_0^{t_c} tp(t)dt = \frac{\int_0^{t_c} tk(t)\exp[-\int_0^t k(t')dt']dt}{\int_0^{t_c} k(t)\exp[-\int_0^t k(t')dt']dt}. \quad (7)$$

For vanishing strain rate, i.e. in the limit of $\dot{\varepsilon} \to 0$, $k(t)$ is a constant, k, and $t_c \to \infty$, Eq. (7) gives the average time as $\bar{t} = 1/k$, which follows the Arrhenius law. However, for the general condition of nonzero strain rate, the result of Eq. (7) will deviate from the Arrhenius behavior.

We emphasize here that the derivations of Eqs. (1)–(7) represent a general formalism that is applicable to a wide range of systems where the reaction rate is time-dependent. Examples include dislocation nucleation under constant strain-rate loading, glass transition at different cooling rates, as well as dislocation flow. In this work we are particularly interested in predicting the variation of flow stress with temperature and strain rate. Because the dislocation will start to glide beyond the residence time $\bar{t}$, we obtain the flow stress by combining Eqs. (2) and (7),

$$\bar{\sigma}_{\text{flow}} = G\dot{\varepsilon}\,\bar{t} = \frac{\int_0^{\sigma_c} \sigma k(\sigma)\exp[-\frac{1}{G\dot{\varepsilon}}\int_0^{\sigma} k(\sigma')d\sigma']d\sigma}{\int_0^{\sigma_c} k(\sigma)\exp[-\frac{1}{G\dot{\varepsilon}}\int_0^{\sigma} k(\sigma')d\sigma']d\sigma}. \quad (8)$$

In summary, once the dislocation migration barrier profile $E(\sigma)$ is obtained, the flow stress of the corresponding slip system can be calculated according to Eq. (8). There is then only one parameter in Eq. (8), the attempt frequency k_0, which we take to be on the order of 10^{12-13} s^{-1}. Although Eq. (8) is developed to give the flow stress of a slip system, the formalism is applicable in general to any activated process described by Eq. (1).

The deformation of bcc metals at low temperature is known to be controlled by the motion of $\frac{1}{2}\langle 111\rangle$ screw dislocations [19], the flow mechanism being three-dimensional (3D) kink nucleation and propagation [17,18,21]. For the purpose of testing Eq. (8), we will examine a short dislocation of length $5\boldsymbol{b}$, $\boldsymbol{b}$ being the Burger's vector, which should glide without kink nucleation. We use a simulation cell of 55 440 atoms, with the dimensions perpendicular to the dislocation line approximately 230 Å × 230 Å. Periodic boundary conditions are applied on the dislocation line and glide directions. The two-dimensional (2D) glide motion in this case is frequently studied to infer the three-dimensional behavior [21]. The embedded-atom method-type potential developed by Mendelev *et. al.* [22] is employed. To benchmark the results obtained using Eq. (8), we performed direct molecular dynamics (MD) simulations on the same system at the high strain rates where MD is known to be valid. The strain-rate conditions, 10^7 and 10^6 s^{-1}, correspond to steady-state dislocation velocities of 22 and 2.2 m/s, respectively. The simulations show that, at low $T < 100$ K, the dislocation moved practically in the same {110} plane, while at higher T frequent cross-slips were observed and the overall motion was a combination of slips in the {110} and {112} planes.

The strain-stress curve for our screw dislocation under static conditions is first shown in Fig. 1(a). Plastic deformation is seen to set in at around 1400 MPa, consistent with the known Peierls stress values [23]. We then determine the glide barriers for the particular model under study using atomistic simulations capable of probing different stress conditions. The nudged elastic band method [24] is one way to map out the glide barrier since the initial and

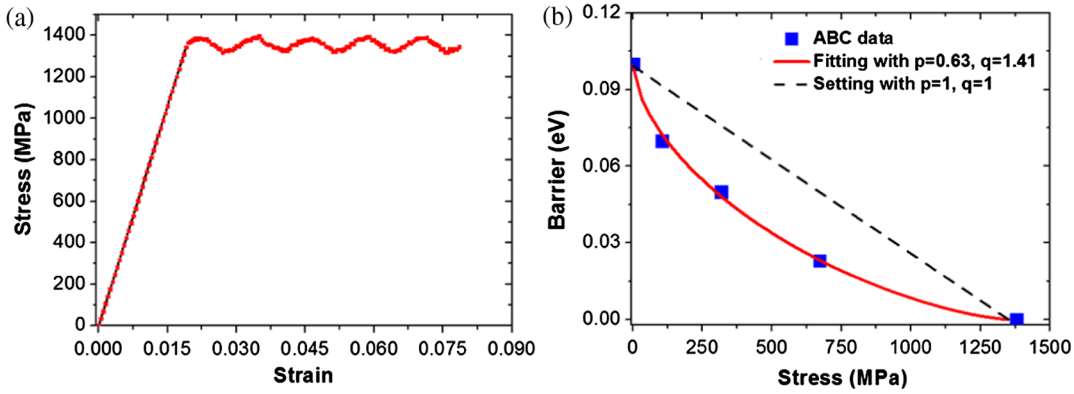

FIG. 1 (color online). (a) Strain-stress curve of the $\frac{1}{2}\langle 111\rangle$ screw dislocation in bcc Fe under static conditions. The corresponding Peierls stress is about 1400 MPa. (b) Activation barrier for the glide motion of $\frac{1}{2}\langle 111\rangle$ screw dislocation as a function of stress. Blue squares represent the calculated data points by the ABC method. The red solid line is a fit to $E(\sigma) = E_0[1 - (\sigma/\sigma_c)^p]^q$ with $p = 0.63$ and $q = 1.41$. The dashed line represents a constant activation volume scenario with $p = 1$ and $q = 1$.

final states of the transition are known. We will use instead an alternative metadynamics sampling method known as autonomous basin climbing (ABC) [25], which does not require knowing the final state. At a given stress state, the method induces the dislocation to migrate to the adjacent energy valley by a series of activation and relaxation steps. As seen in Fig. 1(b), the glide barrier shows a monotonic, though nonlinear, decrease as one may generally expect for a stress-activated process. This is indeed what is known from a recent study of surface dislocation nucleation [15]. To fit the experimental data, a commonly used expression is $E(\sigma) = E_0[1 - (\sigma/\sigma_c)^p]^q$, where E_0 is the activation barrier under zero stress, σ_c the Peierls stress, and (p, q) are the shape parameters [16–18]. For the stress variation determined here by atomistic simulation the fitting parameters have values of $p = 0.63$, and $q = 1.41$, which give a clearly nonlinear behavior for $E(\sigma)$ as seen in Fig. 1(b). The dashed line in Fig. 1(b), on the other hand, denotes the fit with $p = q = 1$, which is the assumption of a constant activation volume with a linear behavior.

The activation barrier $E(\sigma)$ is the only input needed to predict, through Eq. (8), the temperature and strain-rate variations of the flow stress, both of which can be directly compared against experiments. Figure 2 shows the thermal behavior of flow stress for strain rates varying over 10 orders of magnitude, from 10^7 s^{-1} down to 10^{-3} s^{-1}. In the low temperature limit, absence of thermal activation, all flow stresses approach the Peierls stress. As temperature increases, all the flow stresses monotonically decrease and approach zero at essentially room temperature. At a fixed temperature, higher strain-rate loading results in higher flow stress response. Thus any attempt to compare experimental data against MD simulations must take into account the difference in the strain rate.

The symbols in Fig. 2(a) represent the MD results at strain rates of 10^6 s^{-1} and 10^7 s^{-1}. They are in reasonable agreement with the predictions of Eq. (8) using $k_0 = 1.2 \times 10^{12}$ s^{-1}, which matches the Debye frequency satisfactorily. This constitutes a self-consistent test of Eq. (8) with $E(\sigma)$ taken from Fig. 1(b) in the range of strain rates where MD is valid. One can see an increasingly sharp drop of flow stress as the strain rate decreases to the range accessible to conventional experiments. The sharp drop has been known as a significant feature of the thermal activation process; this behavior is not well captured by MD simulations at its characteristic strain rates [15,19]. Figure 2(a) shows that this behavior is at least qualitatively accounted for by the present model.

To probe further the coupled effect of thermal and stress activation, we plot strain rate and reciprocal temperature at constant flow stresses in Fig. 2(b), where a linear relation would indicate adherence to Arrhenius behavior. Non-Arrhenius behavior is seen to set in at high $\dot{\varepsilon}$. Thus a lower effective barrier at high strain rates is indicated.

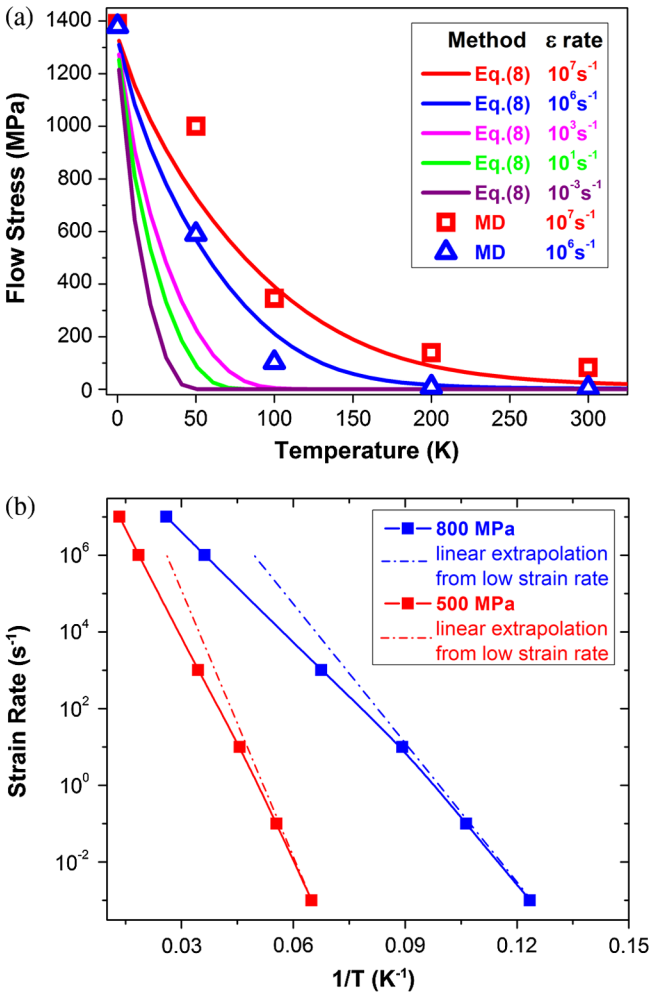

FIG. 2 (color online). (a) The flow stress of the $\frac{1}{2}\langle 111\rangle$ screw dislocation under different strain rate and temperature conditions. The solid lines show the results calculated according to Eq. (8) with the attempt frequency of 1.2×10^{12} s^{-1}. The open squares and triangles represent direct MD simulation results at strain rates of 10^7 s^{-1} and 10^6 s^{-1}, respectively. (b) The relation between strain rate (in logarithmic scale) and $1/T$ at constant flow stress of 800 MPa and 500 MPa. The dashed lines are linear extrapolation from the low strain-rate regime.

The variation of flow stress with strain rate is of fundamental interest in experimental studies of crystal plasticity. Figure 3(a) shows the predicted behavior based on Fig. 2(a) and Eq. (8). Under the limit of infinitely high strain rate, the flow stress approaches the Peierls stress. On the other hand, the flow stress is negatively sensitive to the temperature. In the high temperature limit, the flow stress approaches zero regardless of the strain rate. At low $\dot{\varepsilon}$, the flow stress increases only moderately, but as $\dot{\varepsilon}$ increases, above 10^0 s^{-1} at 50 K, and 10^4 s^{-1} at 100 K, it begins to increase much more strongly.

This upturn behavior can be analyzed in terms of two factors, stress-dependent activation volume, and strain-rate-induced non-Arrhenius behavior. Because of

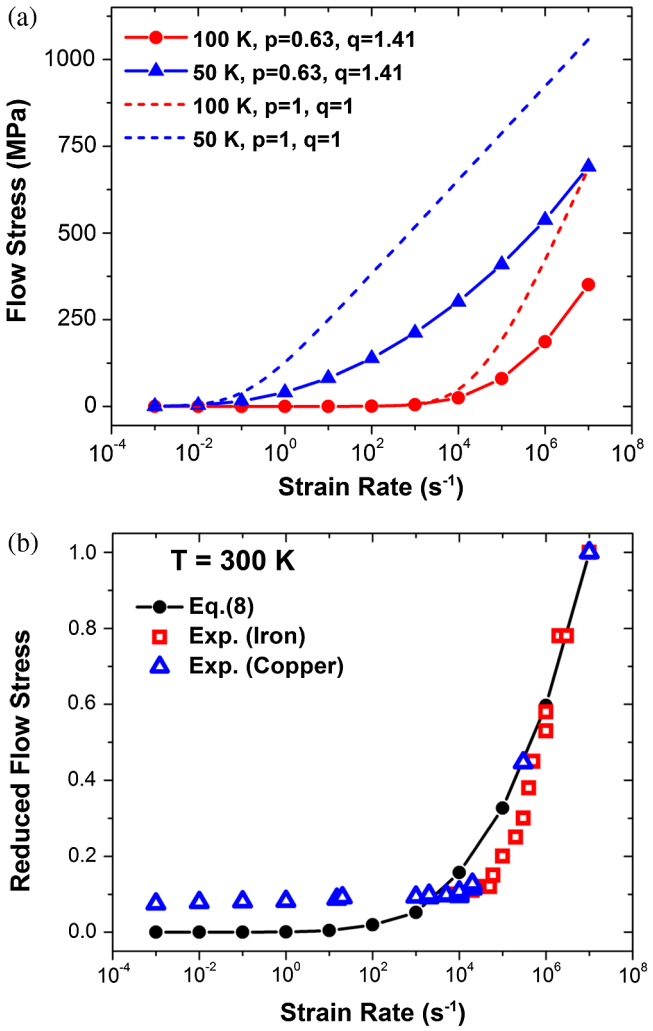

FIG. 3 (color online). (a) The predicted relation between flow stress and strain rate at 50 K and 100 K. The solid symbols and lines are the calculated results for the $\frac{1}{2}\langle 111\rangle$ screw dislocation in bcc Fe with $p = 0.63$ and $q = 1.41$ in $E(\sigma) = E_0[1 - (\sigma/\sigma_c)^p]^q$. The dashed lines are the results for a hypothetical scenario of $p = 1$ and $q = 1$ that corresponds to constant activation volume for the dislocation. (b) Variation of reduced flow stress with strain rate at 300 K. The experimental data on copper (blue triangles) and on iron (red squares) are adapted from Ref. [7] and references therein. The black line represents the results calculated by Eq. (8), with the activation energy profile input from Gordon et al.'s work in Ref. [21] for a long screw dislocation in bcc Fe.

the nonlinear stress dependence of the activation barrier [Fig. 1(b)], the activation volume is very small at high stresses. Such small activation volume leads to a high sensitivity of the flow stress dependence on strain rate [15]. In addition, as derived in Eq. (7), there is a non-Arrhenius behavior due to the strain-rate loading, which also contributes to the upturn in Fig. 3(a). To decouple the two contributions, we remove the nonlinearity of $E(\sigma)$ by setting p and q equal to unity [dashed line in Fig. 1(b)]. Now the only nonlinear factor comes from the strain-rate-induced non-Arrhenius behavior in Eq. (8). As shown in Fig. 3(a), under this condition, the flow stress upturn remains, but the stress is now higher beyond the crossover strain rate. Since the assumption of $p = q = 1$ results in a higher effective barrier and correspondingly a longer residence time, it follows that the flow stress response is higher as well. Our analysis therefore shows the onset of flow stress upturn is to be attributed mainly to the non-Arrhenius behavior induced by strain rate, as described by Eqs. (7) and (8). This result stands in contrast to the previous study of Domain *et al.* [19], which extrapolated the short time-scale simulations to long-term behavior by assuming a linear relation between flow stress σ_{flow} and logarithm of strain rate $\ln\dot{\varepsilon}$.

To compare the predicted upturn behavior quantitatively with experimental data, we adapt the energy profile $E(\sigma)$ for a longer screw dislocation system in bcc Fe calculated by Gordon *et al.* [21] and use it as input into Eq. (8). Figure 3(b) shows the variation of flow stress and strain rate at 300 K, as observed experimentally and predicted by our model. Since the magnitude of flow stress is significantly influenced by the defect microstructures in the experimental specimens [7], the quantitative comparison can only be meaningful after appropriate normalization, e.g., in a previous reduction of the viscosities of various supercooled liquids [26]. Therefore, in Fig. 3(b) we show the reduced flow stress, defined as the ratio of flow stress to its value at the highest strain rate 10^7 s^{-1}, as a function of strain rate. It is seen that both the experiments and our calculation results show a significant flow stress upturn with the critical strain rate in the range of 10^4–10^5 s^{-1}. We regard the quantitative agreement with experiments to be a test of whether the mechanism of the transitional behavior is described correctly. The extent of the agreement suggests Eq. (8) plus $E(\sigma)$ have essentially captured the mechanism for the flow stress upturn behavior. On the other hand, it is known that the flow stress magnitude depends on the local defect microstructure in the material. Experimental specimens have a complex defect microstructure leading to appreciably higher flow stresses (due to, for example, dislocation-obstacle interactions) seen in the experiments compared to the results in Fig. 3(a). It is therefore intriguing that the reduced flow stress predicted by our model in Fig. 3(b) is also quantitatively consistent with experiments from different materials (a ductile one, copper, and a brittle one, iron). We attribute this finding to the fact that the energy barrier for dislocation to climb (glide) over the defects (obstacles) in the material bears a similar stress-activated behavior as the simple dislocation glide represented by the expression $E(\sigma) = E_0[1 - (\sigma/\sigma_c)^p]^q$ that was described above [13]. Thus, Fig. 3(b) demonstrates not only the accuracy of our model and the governing mechanism of flow stress upturn, but also the general applicability of this model regarding

problems of coupled stress and thermal activated processes, beyond simple dislocation glide.

In this work, we present a constitutive model which describes the variation of the plastic flow stress with temperature and strain rate. The model is given by Eq. (8), which involves the specification of $E(\sigma)$, the stress-dependent activation barrier for dislocation mobility. This is the key and the only input needed for the model to predict the temperature and strain-rate behavior shown in Figs. 3(a) and 3(b), respectively, results that are tested against measurements. We show that the coupled effects of thermal and stress activation can be analyzed naturally in the framework of transition state theory (for activated state processes). With respect to the particular phenomenon of the flow stress upturn (Fig. 3), we provide a parameter-free explanation of the transition from thermal- to stress-activation controlled regimes across a critical $\dot{\epsilon}$ range that matches well with experiments, as an alternative to the interpolative models in the literature [1,11,13]. It would be of considerable interest to test whether this model can also help understand the yield strength upturn behavior at high strain rates in glassy solids [27]. Additionally, it is also tempting to provide analogies with other crossover phenomena, for example, the variation of strain rate with applied stress well known in thermal creep, or the classical variation of viscosity with reciprocal temperature in glass transition.

Work supported by the Consortium for Advanced Simulation of Light Water Reactors, an Energy Innovation Hub for Modeling and Simulation of Nuclear Reactors under U.S. Department of Energy Contract No. DE-AC05-00OR22725, while Y. N. O. was also supported by the Division of Materials Sciences and Engineering, U.S. Department of Energy.

*Corresponding author.
byildiz@mit.edu

[1] K. G. Hoge and A. K. Mukherjee, J. Mater. Sci. **12**, 1666 (1977).
[2] W. G. Ferguson, F. E. Hauser, and J. E. Dorn, Br. J. Appl. Phys. **18**, 411 (1967).
[3] A. Kumar, F. E. Hauser, and J. E. Dorn, Acta Metall. **16**, 1189 (1968).
[4] J. D. Campbell and W. G. Ferguson, Philos. Mag. **21**, 63 (1970).
[5] P. S. Follansbee, G. Regazzoni, and U. F. Kocks, in *Mechanical Properties of Materials at High Strain Rates*, edited by J. Harding (Institute of Physics and Physical Society, London, 1984), p. 71.
[6] G. Regazzoni, U. F. Kocks, and P. S. Follansbee, Acta Metall. **35**, 2865 (1987).
[7] R. W. Armstrong, W. Arnold, and F. J. Zerilli, J. Appl. Phys. **105**, 023511 (2009).
[8] G. R. Johnson, J. M. Hoegfeldt, U. S. Lindholm, and A. Nagy, J. Eng. Mater. Technol. **105**, 42 (1983).
[9] F. J. Zerilli and R. W. Armstrong, J. Appl. Phys. **61**, 1816 (1987).
[10] P. S. Follansbee and U. F. Kocks, Acta Metall. **36**, 81 (1988).
[11] D. J. Steinberg and C. M. Lund, J. Appl. Phys. **65**, 1528 (1989).
[12] D. L. Preston, D. L. Tonks, and D. C. Wallace, J. Appl. Phys. **93**, 211 (2003).
[13] B. A. Remington *et al.*, Mater. Sci. Technol. **22**, 474 (2006).
[14] R. W. Armstrong, Acta Metall. **15**, 667 (1967).
[15] T. Zhu, J. Li, A. Samanta, A. Leach, and K. Gall, Phys. Rev. Lett. **100**, 025502 (2008).
[16] U. F. Kocks, A. S. Argon, and M. F. Ashby, in *Progress in Materials Science*, edited by B. Chalmers, J. W. Christian, and T. B. Massalski (Pergamon, New York, 1975), p. 110.
[17] D. Rodney and L. Proville, Phys. Rev. B **78**, 104115 (2008).
[18] D. Rodney and L. Proville, Phys. Rev. B **79**, 094108 (2009).
[19] C. Domain and G. Monnet, Phys. Rev. Lett. **95**, 215506 (2005).
[20] A. F. Voter, in *Radiation Effects in Solids*, edited by K. E. Sickafus, E. A. Kotomin, and B. P. Uberuaga (Springer-Verlag, Berlin, 2007), p. 1–24.
[21] P. A. Gordon, T. Neeraj, Y. Li, and J. Li, Model. Simul. Mater. Sci. Eng. **18**, 085008 (2010).
[22] M. I. Mendelev, S. Han, D. J. Srolovitz, G. J. Ackland, D. Y. Sun, and M. Asta, Philos. Mag. **83**, 3977 (2003).
[23] D. Terentyev, G. Bonny, C. Domain, and R. C. Pasianot, Phys. Rev. B **81**, 214106 (2010).
[24] G. Henkelman and H. Jonsson, J. Chem. Phys. **113**, 9978 (2000).
[25] A. Kushima, X. Lin, J. Li, J. Eapen, J. C. Mauro, X. Qian, P. Diep, and S. Yip, J. Chem. Phys. **130**, 224504 (2009).
[26] C. A. Angell, J. Phys. Chem. Solids **49**, 863 (1988).
[27] J. Rottler and M. O. Robbins, Phys. Rev. E **68**, 011507 (2003).